Probing Short Range Correlations

at the HyperNIS experimental area

List of organizations and participants

Russia: Joint Institute for Nuclear Research – JINR (Dubna)

Israel: Tel Aviv University

USA: FIU, MIT, ODU, PSU

Spokespersons:

Or Hen (MIT), Eli Piasetzky (TAU), Julian Kahlbow (MIT, TAU), Maria Patsyuk (JINR)

Coordinators:

Maria Patsyuk (JINR), Julian Kahlbow (MIT, TAU)

Theoretical Support:

Leonid Frankfurt (TAU), Misak Sargsian (FIU),

Mark Strikman (PSU), Yuri Uzikov (JINR), Alexey Larionov (JINR)

Abstract

We present a two-phase research program aimed at investigating Short-Range Correlations (SRC) at the Joint Institute for Nuclear Research (JINR). In Phase I, which spans the next 2-3 years, our focus will be on conducting measurements in the HyperNIS area. These measurements will involve the use of a polarized deuteron beam from the Booster/Nuclotron and existing detection equipment at JINR. Specifically, we will explore polarized deuteron hard scattering off a liquid hydrogen target, with a focus on SRC kinematics. With a polarized deuteron beam of 6 GeV/c/nucleon momentum we will select interactions with $|t, u| > 1$ $(GeV/c)^2$, and a center-of-mass scattering angle around 90 degrees. A coincidence between the two arms of a dedicated spectrometer will identify two protons resulting from the p(d,2p)n reaction. Simultaneous detection of the recoil partner neutron arising from the deuteron's hard breakup will also be possible. The two-arm spectrometer will be akin to the one used in the 2022 SRC/BM@N measurement. Detection of the recoil neutron will necessitate the incorporation of a neutron detector along the beam. It is important to note that the installation of the required detection systems for Phase I measurements in the HyperNIS experimental area will not disrupt the existing HyperNIS experimental setup.

Phase II of our research, also proposed to be conducted in the HyperNIS area, will focus on exclusive quasi-elastic scattering reactions in inverse kinematics with detection of the recoil fragment/fragments in coincidence. This phase requires extensive preparatory work, encompassing design and engineering efforts within the experimental area, and an investment in equipment.

Both phases are an integral component of the global endeavor led by the international SRC collaboration to study dense nuclear systems and nucleon-nucleon interactions at close proximity, employing various reaction probes such as electrons, real photons, protons, and nuclei.

Table of content

1. Introduction

After the successful campaigns conducted at the BM@N experimental area in 2018 and 2022, we present here our proposal for continuing the SRC (Short-Range Correlations) studies at JINR. To begin, we will provide a brief overview of the 2018/2022 measurements, followed by the introduction of our proposed program.

The Phase I measurements will be carried out at the HyperNIS area, utilizing a polarized deuteron beam and making use of the existing equipment at JINR. Pending approval, we believe that Phase I can be completed within the next 2-3 years.

The second phase of our project, Phase II, is dedicated to exclusive SRC studies. This phase will also take place at the HyperNIS area but will require additional research and investment in terms of design and equipment, and adjustment of the experimental area for those measurements.

Both phases are part of a broader SRC program conducted by our international collaboration. This study spans various accelerator laboratories across the globe using electrons, real photons, protons, and nuclei as probes. The primary objective of this SRC study is to enhance our understanding of the nuclear many-body system and nucleon-nucleon interactions at short distances, characterized by high nuclear densities, large relative momenta, and high virtuality.

2. Measurements in 2018 and 2022

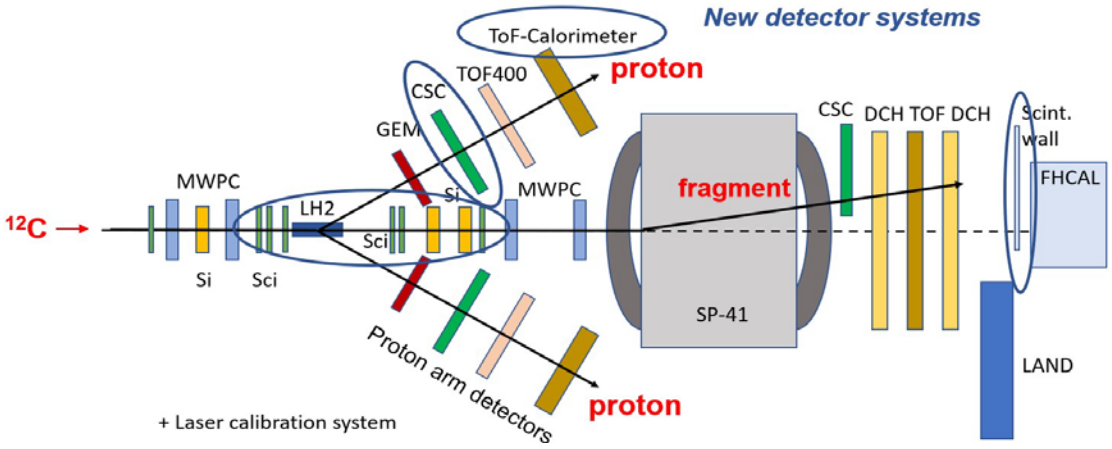

FIG. 1: The BM@N spectrometer setup for the second SRC measurement in 2022. The reaction of interest is $^{12}C + p \rightarrow 2p + X$. New detector systems added and modified after the 2018 measurement are marked with blue ellipses.

The initial SRC experiment at JINR in 2018 employed the BM@N spectrometer, a 4 GeV/c/nucleon carbon beam, a liquid hydrogen target, and two dedicated detector arms. This pilot study served as a fundamental proof of concept for investigating Short-Range Correlations (SRC) in hard inverse kinematics with a high-energy nuclear beam. The results of this pioneering experiment were published in Nature Physics [1].

The second SRC experiment was developed to significantly enhance the statistical data by an order of magnitude. Its objectives included obtaining absolute cross-sections for quasi-free (QF) single proton removal and examining SRC pairs in carbon-12, encompassing the fragmentation of the residual A-2 system after the SRC removal. To achieve these aims, substantial improvements were made to the experimental setup, as depicted in Fig. 1. This involved the addition of a new Time-of-Flight (TOF) detector array and a set of novel scintillator trigger counters. Furthermore, a laser system was integrated to enable the simultaneous calibration of all scintillator detectors without the beam. The data acquisition process spanned two weeks following a week-long calibration period. Presently, data analysis is in progress, and preliminary results are illustrated in Fig. 2 up to the identification of quasi-elastic events, reproducing results from the 2018 measurement on a limited data set.

Figure 2a displays the identification of incoming carbon-12 ions, while figure 2b shows the fragment spectrum. Notably, figure 2c exhibits the reconstructed reaction vertex, which clearly delineates the shape of the liquid hydrogen (LH) target. Figures 2d+e show the identification of quasi-elastic (QE) events based on proton opening angle and missing energy as reconstructed from the two-arm spectrometer. The coincidence with the 11B fragment (Fig. 2e) suppresses initial-/final-state interactions and allows to cleanly separate QE events. The corresponding missing momentum distribution is shown in Fig. 2f where, again, the fragment coincidence removes the high-momentum tail that originates from FSI effects. This reproduces our 2018 results.

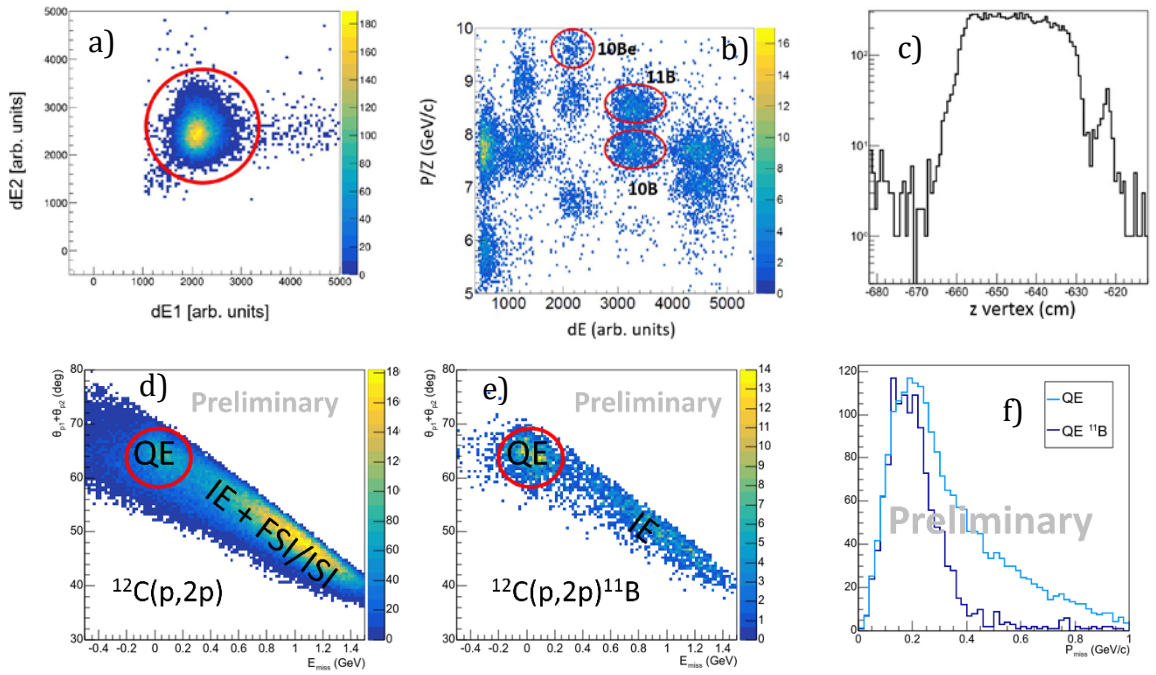

FIG. 2: Preliminary results from the measurement performed in March 2022: a) identification of the incoming ^{12}C ions using two beam scintillator counters, b) identification of the final state ion fragments, c) reconstruction of the interaction vertex coordinate along the beam using tracks in the two arms. d+e) Identification of quasi-elastic (QE) events, separating from inelastic and final-state interactions (IE, FSI), without and with ^{11}B fragment coincidence. f) Preliminary missing momentum distribution for $^{12}C(p,2p)^{11}B$, for a limited data set.

The dedicated SRC detectors were moved from the BM@N area and stored in the HyperNIS area in Bld. 205. The current proposal describes the continuation of the SRC program at the HyperNIS area using those detectors.

3. Phase 1: Polarized deuteron beam measurements in SRC kinematics

3.1 Deuterons as surrogate for two-particle correlations in nuclei

In atomic nuclei, nucleons often pair up with significant relative momenta while having small center-of-mass (CM) momenta. Here, "large" and "small" are relative to the Fermi momentum (k_F) of the nucleus. These special pairs are referred to as short-range correlated (SRC) pairs [2-4]. SRC pairs provide valuable insights into several aspects of nucleon and nuclear physics, including the distribution of high momenta within nuclei, the short-distance features of the nucleon-nucleon interaction, and the inner quark-gluon structure of bound nucleons [42,5,9,23,28].

Over the past decade, we have made remarkable progress in understanding SRCs through exclusive electron hard knockout reactions, namely A(e,e′N) and A(e,e′pN) [5-9], where "N" stands for a neutron or proton. These experiments were conducted on selected nuclei (A = ^{4}He, C, Al, Fe, and Pb). In these reactions, electrons interacted with protons or neutrons in the target nucleus, resulting in high-momentum transfers (QF reaction with $Q^2 > 1.5$ $(GeV/c)^2$). This led to the knockout of high-momentum nucleons and, in some cases, the emission of correlated recoil nucleons.

Exclusive measurements of SRC pair breakup reactions using electrons [5-7, 10-13], and also protons [11, 12], on various nuclei revealed the following findings:

- Protons knocked out with high missing momentum ($300 \leq p_{miss} \leq 600$ MeV/c, where $\vec{p}_{miss} = \vec{p}_{probe} - \vec{q}$) almost always have an associated recoil nucleon with momentum that balances the missing momentum.
- These recoil nucleons are predominantly neutrons. Neutron-proton (np) SRC pairs are nearly 20 times more common than proton-proton (pp) SRC pairs, and by extension, neutron-neutron (nn) pairs. This phenomenon is termed "np-dominance," as shown in Fig. 3.
- The relative momenta of SRC nucleons within a pair, as reconstructed from the missing and recoil nucleon momenta, exceed the Fermi momentum (k_F), while the center-of-mass momenta are consistent with the total momenta of two mean-field nucleons (typically, k_F is around 250 MeV/c for medium to heavy nuclei).

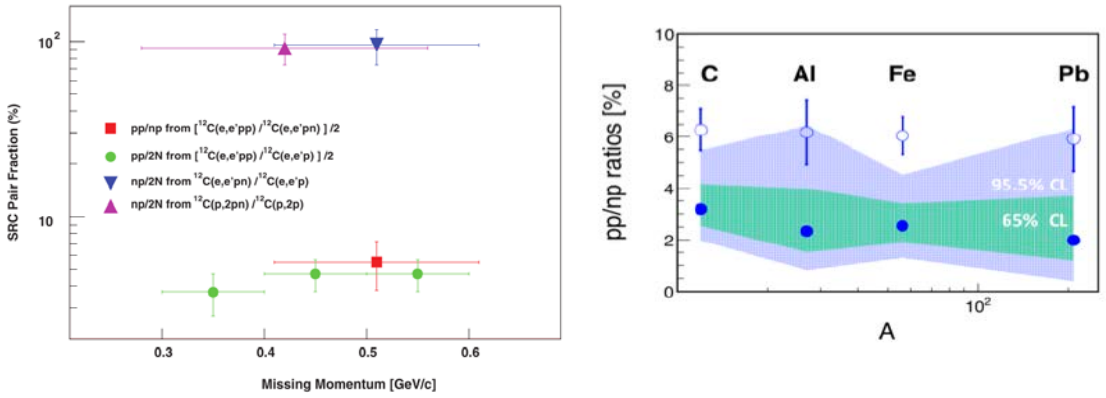

FIG. 3: Results from various A(e, e′p) and A(e, e′pN) measurements, A stands for nuclei from ^{4}He to Pb. Left: the fraction of knocked-out protons with a correlated neutron (triangles) and proton partner (green circles), and the ratio of np- to pp-SRC pairs (red square) in C, extracted from (p, 2pn) [11, 12] and (e, e′pN) [5-7, 10-13] measurements; Right: the ratio of pp to pn SRC pairs for different nuclei from (e, e′Np) measurements [19] without (points) and with (bands) reaction mechanism corrections. The inner and outer bands represent the 68% and 95% confidence limits of the extracted ratios, respectively.

From a theoretical perspective, the prevalence of np-SRC pairs over pp-SRC pairs in nuclei has been extensively examined using advanced ab-initio many-body calculations [13-18]. These calculations underscore the dominance of np pairs at relative pair momenta greater than 300 MeV/c. By exploring various configurations of the nucleon-nucleon interaction, including the presence or absence of a substantial tensor force, we have identified the unique role of the latter in the relevant momentum range [14]. Essentially, most of the SRC pairs resemble deuteron-like states within the nucleus.

The 'Generalized Contact Formalism' (GCF) approach, as illustrated in Fig. 4, leverages the underlying dynamics of short-range correlation (SRC) pairs within nuclei [20,21]. In this framework, the many-body wave function at short distances decomposes into two key components. First, there is a universal two-body function, which exclusively relies on the relative momentum of the pair. Second, there is a many-body function with characteristics reminiscent of a mean field, dependent on the center-of-mass momentum (p_{cm}) of the pair.

This decomposition arises from a separation of scales within the nuclear system. There is a marked distinction between the high-momentum, short-distance scale that governs the pair relative momentum (p_{rel}), and the lower-momentum, longer-distance scale that

influences the collective many-body dynamics, determining the total number of pairs and their center-of-mass momentum distribution.

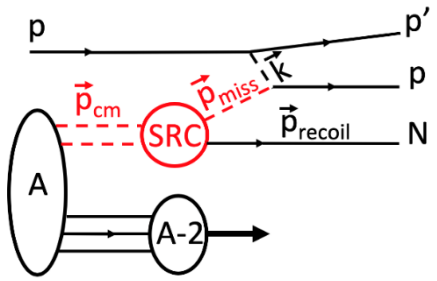

FIG. 4: Diagrammatic representation and kinematics of the triple-coincidence A(p,2pN) reaction within the SRC breakup model. Dashed red lines represent off-shell particles, and the solid lines represent detected particles.

This formalism has been rigorously benchmarked against state-of-the-art VMC and Cluster-VMC calculations for nuclei ranging from ^{4}He to ^{40}Ca, both in terms of momentum and coordinate space [22]. The results of this phenomenological approach demonstrate a high degree of agreement with ab initio calculations, underlining its validity and utility in the study of nuclear dynamics [23,24].

Within the GCF the A(e,e'NN) plane wave cross-section can be expressed as [20,21,24]:

$$\frac{d^8\sigma}{dQ^2 dx_B d\phi_e d^3_{p_{cm}} d\Omega_{rec}} = K \times \sigma_{eN} \times n(p_{CM}) \times [\sum_\alpha C_\alpha \cdot |\tilde{\varphi}^\alpha(|\vec{p}_{CM} - 2\vec{p}_{rec}|)|^2], \qquad \text{Eq. 1}$$

with a similar expression for the proton scattering case. The subscripts 'N' and 'rec' stand for the leading and recoil nucleons, respectively. K is a Jacobean term, σ_{eN} is the off-shell electron-nucleon cross-section, and α represents the quantum numbers of SRC pairs. $\tilde{\varphi}^\alpha$, $n(p_{CM})$, and C_α, respectively, describe the relative and center-of-mass motion of SRC pairs as well as their overall abundances, such that:

- $\tilde{\varphi}^\alpha$ are universal SRC pairs relative momentum distributions, obtained by solving the zero-energy two-body Schrödinger equation of a NN pair in quantum state α using an input NN potential model
- $n(p_{CM})$ is the SRC pair center-of-mass momentum distribution, given by a three-dimensional Gaussian with a width of 150 ± 20 MeV/c [25]
- C_α are nuclear contact terms that determine the relative abundance of SRC pairs in quantum state α and are obtained from analysis of ab-initio many-body calculations of two-nucleon densities. These contact terms are also consistent with the values extracted from data [26-28,22]

3.2 Research objectives and expected significance.

Studying nuclear structure at short distances necessitates a relativistic description of the bound system. However, there is no single prescribed method for achieving this, and the acquisition of polarization data on the deuteron is crucial for understanding the relativistic effects involved [1,2,29,30,33].

The presence of the D-wave component in the deuteron arises from the deuteron's finite quadrupole moment, which is directly associated with the tensor component of the nucleon-nucleon (NN) interaction. The tensor force does not conserve the individual spin (S) or orbital angular momentum (L) but only the total angular momentum (J). As a result, it permits a mixing of the primarily spherically symmetric S state with configurations featuring L = 2 D-state.

Modern NN interaction potentials provide predictions for the overall probability of the D-wave in the deuteron, ranging from approximately 4.87% (e.g., CDBonn) to 5.76% (e.g., AV18) [31,32]. While this difference may appear small, these parameterizations project substantially different strengths at high momenta, particularly above 400 MeV/c, which is primarily associated with the SRC D component [33].

The knowledge of the S/D (S-wave/D-wave) ratio at large momenta is closely linked to the NN short range tensor force that is also responsible to the strong SRC np-dominance [7,11,23]. The S/D ratio is not an observable; however, it can be constrained within a given calculations by comparing to data. It is currently insufficiently constrained by the available data at the high momentum tail of the deuteron wave function. Proposed measurements of tensor polarization observables at SRC kinematics like the asymmetry A_{zz} [34-38],

$$A_{zz} = \frac{(\sigma_- + \sigma_+ - 2\sigma_0)}{\sigma_{unpol}},$$

with the yields σ for the different tensor polarization states (-, +, 0), relate in PWIA to the deuteron composition [36]:

$$A_{zz} \sim \frac{\frac{1}{2}w^2(k) - u(k)w(k)\sqrt{2}}{u^2(k) + w^2(k)}$$

where u(k) is the S-state wave function and w(k) is the D-state wave function. This non-relativistic expression was shown to be correct also within the light front formalism by choosing appropriate value for k, see details in [38]. We propose here to collect data that is highly sensitive to the D/S ratio in the high-momentum tail as discussed below. Theoretical calculations and predictions with final-state interactions (FSI) are in progress for the proposed reaction and kinematics [37-39].

The dominant two-body SRC pairs are the neutron-proton pairs with quantum numbers of a deuteron. Measuring the polarization states in the deuteron with the unique polarized deuteron beam available at JINR is crucial for understanding SRC in nuclei. Most important advancement in this respect is the possibility of measuring polarization states at fixed and large values of internal momenta of the nucleons in the deuteron.

These studies will allow to address several questions:

- What is the deuteron wave function below the inelastic threshold?
- How do polarization states impact sensitivity to relativistic effects?
- Are there non-nucleonic components that can be observed using polarization [48]?

3.3 Rate estimate and expected uncertainties

The highest attainable beam momentum for polarized deuterons at the HyperNIS area is 6 GeV/c/nucleon, with a maximum beam intensity of 10^{10} ions per spill. We can generate various polarization modes (tensor, vector, unpolarized) by alternating the polarization for each spill. However, due to limitations imposed by our detectors and other experimental constraints, we anticipate that a realistic beam rate for data collection with our current setup would be approximately 10^6 ions per second.

Our plan involves continuing the use of the cryogenic liquid hydrogen target that was employed in the last SRC measurement at BM@N in 2022 at the HyperNIS area. The experimental setup (as shown in Fig. 5) for studying deuteron breakup reactions necessitates a two-arm spectrometer and a downstream neutron detector along the beam. The required equipment is already available at JINR, having been utilized during the last SRC measurement period in 2022. But we will need to upgrade the electronic readout systems to meet our current research needs.

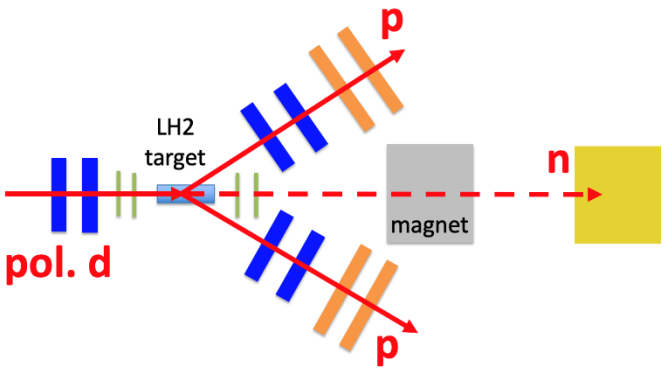

FIG. 5: Schematic of the experimental setup for the studies with polarized deuteron beam. The key components are: Scintillator Beam Counters (Green): Positioned both before and after the target, these scintillator detectors serve the dual purpose of measuring the beam's start time and monitoring its charge. These detectors play a vital role in initiating and tracking the beam as it progresses through the experimental apparatus. Position sensitive Detectors (Blue): These detectors facilitate the precise reconstruction of the trajectory of the incoming beam and the protons emitted. Timing Detectors (Orange): The orange detectors are crucial for identifying the signal protons and determine their momenta. Neutron Detector (Yellow): Positioned downstream, the neutron detector is used to measure recoil neutrons.

With the incident beam rate and setup described above, we estimate that the trigger rate will be approximately 4 kHz. This estimate is based on the total proton-proton (pp) and proton-neutron (pn) cross-sections, considering a 30 cm liquid hydrogen target. Additionally, it assumes that each arm, covering about 4% of the acceptance, can independently trigger the data acquisition system (DAQ).

To estimate the rate of events relevant to the SRC study, we run realistic simulations using an event generator based on the GCF (see above) and request in the simulation-data analysis:

- $|t|$ & $|u| > 1$ GeV^2
- $60° < \theta_{cm}$
- Two-arm acceptance: $20^0 < \theta_{lab} < 45°$; $-20° < |\varphi_{lab}| < 20°$
- $p_{miss} > 0.25$ GeV/c.

The deuteron wave function falls strongly as a function of the relative momentum between the nucleons, see Fig. 6. The obtained simulated p_{miss} distribution using the AV18 deuteron wave function, a data-based pp cross section parametrization, and the

constraints as listed above, is shown in Fig. 7 (right). Also shown is the expected proton distribution in each arm (Fig. 7, left).

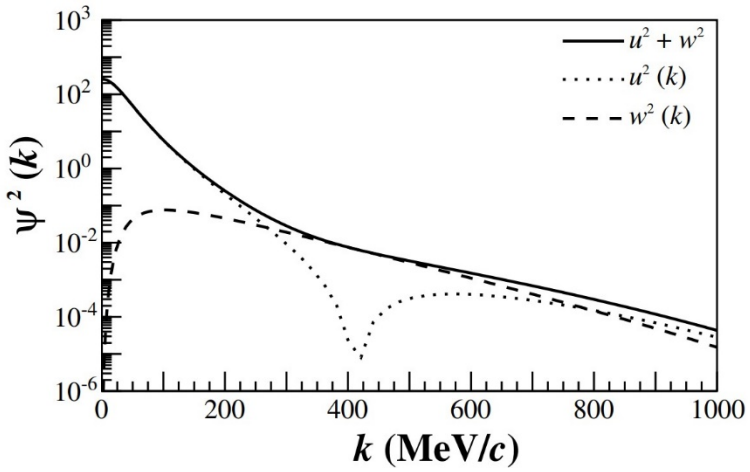

FIG. 6: The AV18 deuteron wave-function. The full wavefunction (solid) has contributions from the D-state (dashed) and S-state (dotted).

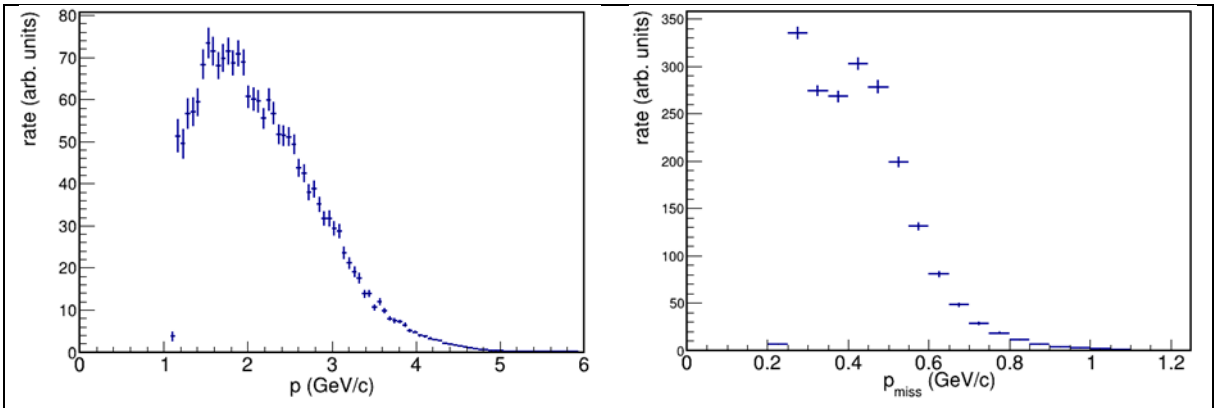

FIG. 7: The simulated distribution of proton momentum in each arm (left) and the missing momentum p_{miss} distribution (right) as to be measured in d(p,2p).

For a beam intensity of 10^6 deuterons/sec the number of expected events that passed the cuts above and two weeks of running is summarized in Table 1. Assuming 25% σ+, 25% σ-, and 50% σ0 polarization, the statistical uncertainties for A_{ZZ} for the p_{miss} bins is also shown below in Table 1.

Table 1: Rate estimates for d(p,2p) (*) for 10^6 deuterons/sec, 50% duty cycle, and 2 weeks running.

p_{miss} bin (GeV/c)	Number of events	A_{zz} stat. uncertainty
0.25 – 0.30	81,030	0.007
0.30 – 0.35	66,220	0.007
0.35 – 0.40	64,820	0.007
0.40 – 0.45	73,200	0.007
0.45 – 0.50	67,310	0.007
0.50 – 0.55	48,050	0.009
0.55 – 0.60	31,690	0.010
0.60 – 0.65	19,390	0.013
0.65 – 0.70	11,530	0.017
0.70 – 0.75	6,800	0.023
0.75 – 0.80	4,350	0.028
0.80 – 0.85	2,620	0.037
0.85 – 0.90	1,510	0.048
0.90 – 0.95	880	0.063
0.95 – 1.00	460	0.087
Total	479,860	

Figure 8 shows calculations by Misak Sargsian and Mark Strikman [38], and Yuri Uzikov together with fictitious data and stat. uncertainties (at high momentum) expected in two weeks of beam on target. The figure demonstrates the sensitivity of the A_{ZZ} calculation to the relativistic formalism (Light cone LC [41] vs. virtual nucleon VNA [40]) and different deuteron wave functions (CD Bonn and Paris potentials). The expected statistical uncertainties show that with a reasonable beam time there are no statistical limitations to distinguishing between different models.

The large acceptance in terms of the (p,2p) missing momentum and the recoil neutron longitudinal and transverse components (α, p_T) will allow us to select and compare events which suppress FSI and others with relatively large FSI to study this important effect. The detailed selections will be finalized using our simulation and the calculations mentioned above [37,38] after the latter will be available.

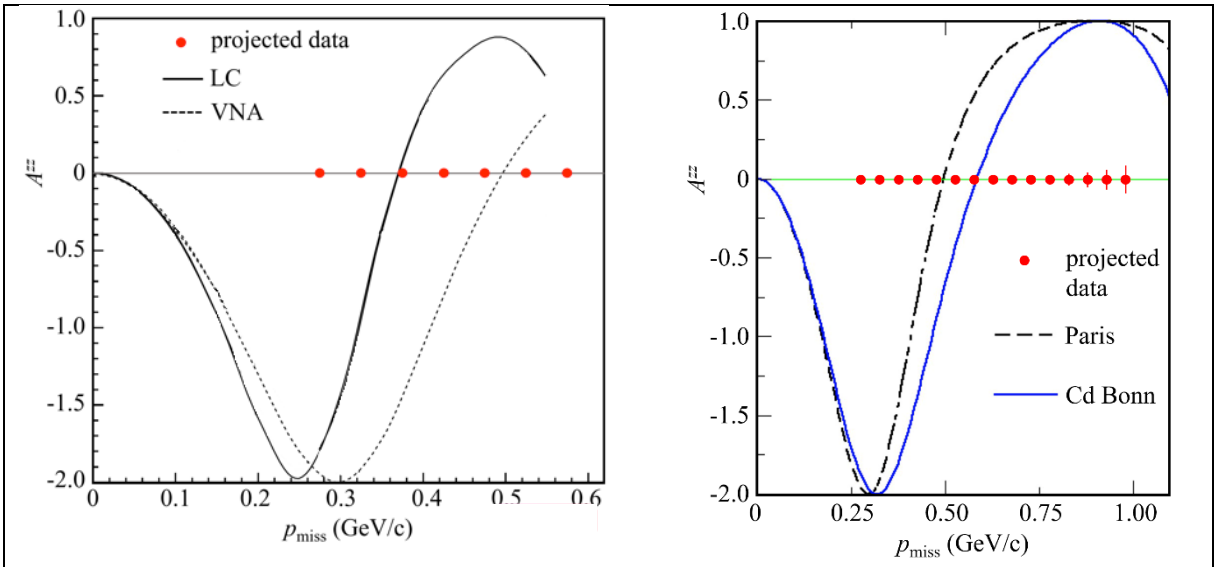

FIG. 8: A_{ZZ} as a function of p_{miss} for two relativistic formalisms, light cone (LC) and virtual nucleon (VNA) (left) and for two different nuclear potentials (right). The projected data is shown by the red dots, the expected statistical uncertainties are often smaller than the points shown.

4. Phase 2: Exclusive SRC measurements

We propose to continue at JINR our international program aimed at investigating SRC effects [42,43] with the primary objective of understanding cold, dense nuclear matter [44,7]. The unique, high-energy ion beams, in conjunction with the dedicated SRC/HyperNIS setup, provide us with means to further explore hard quasi-elastic nucleon knockout from the beam ions in an inverse kinematics setting in coincidence with the residual fragment/fragments.

4.1 Physics goals

Cutting-edge in the SRC research field is the exploration of three-nucleon SRCs [45-47]. These investigations are of paramount importance for gaining precise insights into nuclear structure and nucleon-nucleon interactions. One key advantage of JINR in the pursuit of 3N-SRCs lies in the significantly larger cross-section of proton-proton (pp) scattering when compared to electron-proton (ep) scattering. This expanded cross-section provides a favorable environment for the search for three-nucleon SRCs. The inverse kinematics that allows to identify the A-3 residual system is also an advantage to be utilized in the search for 3N SRC signals.

To carry out studies on 3N-SRCs successfully, specific technical requirements must be met. These requirements include a high-intensity carbon-12 beam, with a rate of 10^7 particles per second and a momentum of approximately 3.5 GeV/c per nucleon.

4.2 Concept for HyperNIS area setup

The conceptual setup for studying SRC at HyperNIS is depicted in Fig. 9. This configuration encompasses both pre-existing components and novel additions:

- The inclusion of a second analyzing magnet significantly enhances the overall resolution for isolated ion fragments.
- A two-arm spectrometer is integrated, comprising two stations of coordinate detectors (GEM and CSC) and a substantial TOF-calorimeter on each arm. This system is purpose-built for track reconstruction of the ejected protons and precise measurement of their momenta.

- Coordinate detectors located between the two magnets and downstream serve the critical function of detecting, identifying, and measuring the momentum of the final-state and recoil ions.

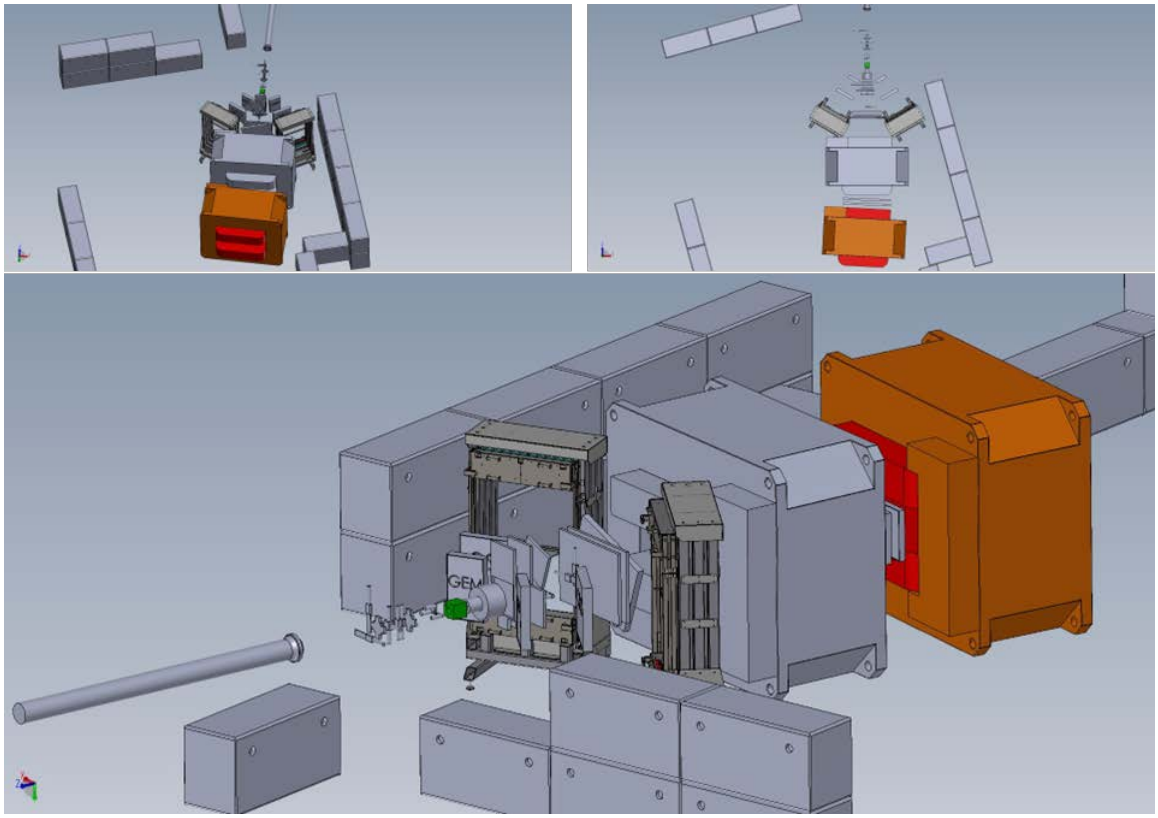

FIG. 9: A CAD model showing different views of the conceptual design of the combined spectrometer for two experiments: HyperNIS and SRC. The major modifications for the SRC experiment are the second dipole magnet (shown in orange) and the two-arm spectrometer located upstream the magnets. These SRC additions are compatible with the HyperNIS setup.

These modifications to the original HyperNIS setup can be seamlessly incorporated without significant disruption to existing equipment, thereby facilitating the concurrent operation of multiple experiments in the same area.

However, the installation of the second dipole magnet necessitates engineering assessments and preparatory work, including floor reinforcement in the HyperNIS area. These tasks are time-consuming, and initiating this work ahead of the final proposal, which will be based on the 2022 results pending approval, is contemplated.

Regarding detector availability, TOF-calorimeter detectors with Front-End Electronics (FEE) are repurposed from the SRC/BM@N setup, while the coordinate detectors for the

arms may be sourced locally at LHEP. However, the coordinate detectors situated between and downstream of the magnets will require manufacturing. Notably, the Data Acquisition (DAQ) system is not yet in place.

The maximum attainable beam momentum for ion beams at the HyperNIS area is 9 GeV/c/charge, equivalent to 4.5 GeV/c/nucleon for carbon beams. The SRC measurement calls for a beam momentum within the 3-3.5 GeV/c/nucleon range. Furthermore, accommodating ion beams with an intensity of up to 10^7 ions/s necessitates upgrades to radiation protection measures in the HyperNIS area. It is important to note that we intend to continue utilizing the cryogenic liquid hydrogen target previously employed in the SRC measurements at BMN in 2022 at HyperNIS.

4.3 Preliminary simulation studies

We conducted a preliminary simulation study for the HyperNIS setup. Assuming a carbon-12 beam we estimated the momentum resolution for fragments emitted along the beam and the geometrical acceptance of the two magnets.

In the BmnRoot software, the BM@N analyzing magnet (SP-41) was adapted to match the SP-40 magnet used at the HyperNIS area. The SP-40 magnet's pole length is 1.5 meters. We scaled the magnetic field map to align with the working magnetic field of 0.6 T (at the highest possible working current of 1100 A). We introduced a second identical magnet in the simulation, with a center-to-center distance of 375 cm. This second magnet was rotated by 4 degrees relative to the first magnet and the global z-axis to enhance the transport of charged fragments (see Fig. 10).

The particles are generated at 550 cm from the center of the first magnet. The trajectories of the fragments, as measured by the silicon detectors upstream of the magnets and the generic detector stack downstream of the magnets, are utilized to derive the P/Z (momentum per charge) ratio using a Multidimensional Fit reconstruction. The two straight portions of the particle trajectory are used as input for a simulation-based approach. We assumed spatial uncertainties of 50 μm for the silicon detectors and 200 μm for the generic detector stack.

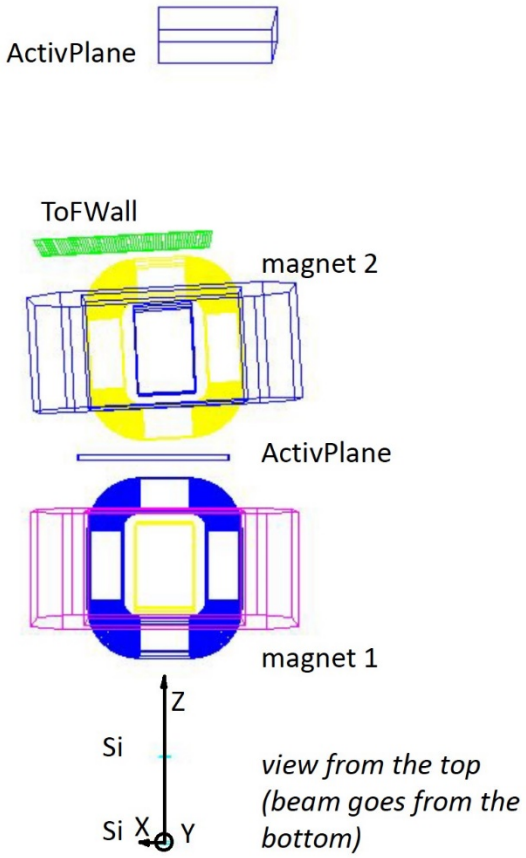

FIG. 10: A top-down view of the simplified experimental setup, with the beam entering from bottom to top. The two SP-40 magnets are labeled as magnet 1 and magnet 2. The active detector system comprises two silicon detectors upstream of the magnets and a generic detector stack downstream of the magnets.

To estimate the momentum resolution for carbon-12 and helium-6 ions (as an extreme P/Z ratio), we used a beam with a circular spot (radius of 4 cm) and a direction defined by Gaussian distributions of px and py with a standard deviation of 150 MeV/c (equivalent to 5 mrad). The absolute momentum spread was defined as (P / 1.1, P * 1.1), where P is the nominal momentum value. The resulting momentum resolutions are presented in Table 2. For comparison, the experimentally achieved momentum resolution in the 2018 SRC experiment at JINR, conducted at the BM@N setup, was 1.6%.

Table 2: The simulated momentum resolution for different ion species.

Ion	Momentum P [GeV/c/nucleon]	standard deviation σ (GeV/c)	σ/P [%]
^{12}C	3.5	0.25	0.6
^{12}C	2.5	0.16	0.55
^{6}He	3.5	0.13	0.9
^{6}He	2.5	0.18	0.8

The primary factor affecting the geometrical acceptance of secondary particles traveling along the beam is the vertical acceptance of the SP-40 magnets. Each SP-40 magnet has dimensions of 3 m along the beam. Considering a 1-meter passageway between the magnets, the total length of the two magnets along the beam is 7 m. The two-arm spectrometer should be positioned upstream of the first magnet, with an arm length of approximately 5 m. This results in a total distance from the target to the exit of the second magnet of about 12 m.

The current vertical opening of the second SP-40 magnet is 40 cm but it can be increased. The geometrical acceptance, based on the magnet opening, is quite limited, as listed in Table 3. The horizontal acceptance is determined by the horizontal dimension of the magnet opening, which is 2.6 m. The acceptance in the horizontal direction for target particles is then 6.5 degrees.

Table 3**:** Geometrical acceptance in the vertical direction for particles originating in the target, for different vertical openings of the second SP-40 magnet.

vertical acceptance of the magnet [m]	vertical geometrical acceptance [degrees]
0.4	1.01
0.5	1.26
0.68	1.73

References

[1] M. Patsyuk et al. (BM@N Collaboration), Nature Physics 17, 693 (2021).

[2] L. Frankfurt, M. Strikman, Phys. Rep. 76, 217 (1981).

[3] L. Frankfurt, M. Strikman, Phys. Rep. 160, 235 (1988).

[4] C. Ciofi degli Atti, Phys. Rep. 590, 1-85 (2015).

[5] O. Hen et al., Science 346, 614 (2014).

[6] I. Korover et al. (JLab Hall A), Phys. Rev. Lett. 113, 022501 (2014).

[7] R. Subedi et al., Science 320, 1476 (2008).

[8] O. Hen et al. (CLAS), Phys. Lett. B 722, 63 (2013).

[9] M. Duer et al. (CLAS), Nature 560, 617 (2018).

[10] R. Shneor et al. (JLab Hall A), Phys. Rev. Lett. 99, 072501 (2007).

[11] E. Piasetzky et al., Phys. Rev. Lett. 97, 162504 (2006).

[12] A. Tang et al., Phys. Rev. Lett. 90, 042301 (2003).

[13] C. Ciofi degli Atti, Phys. Rept. 590, 1 (2015).

[14] R. Schiavilla et al., Phys. Rev. Lett. 98, 132501 (2007).

[15] M. Sargsian et al., Phys. Rev. C71, 044615 (2005).

[16] M. Alvioli, C. Ciofi degli Atti, H. Morita, Phys. Rev. Lett. 100, 162503 (2008).

[17] M. Alvioli, C. Ciofi degli Atti, H. Morita, Phys. Rev. C 94, 044309 (2016).

[18] M. Alvioli et al., Phys. Rev. C 85, 021001 (2012).

[19] M. Duer et al. (CLAS), Phys. Rev. Lett. 122, 172502 (2019).

[20] R. Weiss, B. Bazak, N. Barnea, Phys. Rev. C 92, 054311 (2015).

[21] R. Weiss, R. Cruz-Torres et al., Phys. Lett. B 780, 211-215 (2018).

[22] R. Cruz-Torres et al., Nature Physics 17, 306-310 (2021).

[23] A. Schmidt et al. (CLAS), Nature 578, 540-544 (2020).

[24] J. Pybus et al., Phys. Lett. B 805, 135429 (2020).

[25] E. O. Cohen et al. (CLAS), Phys. Rev. Lett. 121, 092501 (2018).

[26] K. Sh. Egiyan et al. (CLAS), Phys. Rev. C 68, 014313 (2003).

[27] N. Fomin et al., Phys. Rev. Lett. 108, 092502 (2012).

[28] B. Schmookler et al. (CLAS), Nature 566, 354-358 (2019).

[29] L. Frankfurt, M. Strikman, Nucl. Phys. B 148, 107-140 (1979).

[30] W. W. Buck, Franz Gross, Phys. Rev. D 20, 2361 (1979).

[31] R. Machleidt, Phys. Rev. C 63, 024001 (2001).

[32] R. B. Wiringa, V. G. J. Stoks, R. Schiavilla, Phys. Rev. C 51, 38 (1995).

[33] L. Frankfurt, M. Strikman, Nucl. Phys. A 405, 557-580 (1983).

[34] I. Paschier et al., Phys. Rev. Lett. 88, 102302 (2002).

[35] E. Long, J. Phys.: Conf. Ser. 543, 012010 (2014).

[36] L. Frankfurt et al., Z. Phys. A352, 97 (1995); Phys. Lett. B 369, 201 (1996).

[37] A. B. Larionov, Phys. Rev. C 107, 014605 (2023).

[38] M. Sargsian, M. Strikman, J. Phys. Conf. Ser. 543, 012009 (2014).

[39] Alexey Larionov, private communication.

[40] L. Frankfurt et al., Phys. Rev. C 48, 2451 (1993).

[41] M. M. Sargsian, Phys. Rev. C 82, 014612 (2010).

[42] O. Hen et al., Rev. Mod. Phys. 89, 045002 (2017).

[43] J. Arrington, N. Fomin, A. Schmidt, Ann. Rev. of Nucl. and Part. Sc. 72, 307-337 (2022).

[44] L. Frankfurt, M. Sargsian, M. Strikman, Int. J. of Mod. Phys. A 23, 20 (2008).

[45] M. M. Sargsian et al., Phys. Rev. C 100, 044320 (2019).

[46] R. Weiss, S. Gandolfi, Phys. Rev. C 108, L021301 (2023).

[47] D. B. Day et al., Phys. Rev. C 107, 014319 (2023).

[48] M. Sargsian, F. Vera, Phys. Rev. Lett. 130, 112502 (2023).